

Evidence for superconducting gap nodes in the zone-centered hole bands of KFe_2As_2 from magnetic penetration-depth measurements

K. Hashimoto¹, A. Serafin², S. Tonegawa¹, R. Katsumata¹, R. Okazaki¹, T. Saito³, H. Fukazawa^{3,5}, Y. Kohori^{3,5}, K. Kihou^{4,5}, C. H. Lee^{4,5}, A. Iyo^{4,5}, H. Eisaki^{4,5}, H. Ikeda¹, Y. Matsuda¹, A. Carrington², and T. Shibauchi¹

¹Department of Physics, Kyoto University, Sakyo-ku, Kyoto 606-8502, Japan

²H. H. Wills Physics Laboratory, University of Bristol, Tyndall Avenue, Bristol, UK

³Department of Physics, Chiba University, Chiba 263-8522, Japan

⁴National Institute of Advanced Industrial Science and Technology (AIST), Tsukuba, Ibaraki 305-8568, Japan

⁵JST, Transformative Research-Project on Iron Pnictides (TRIP), Chiyoda, Tokyo 102-0075, Japan

(Dated: September 17, 2018)

Among the iron-based pnictide superconductors the material KFe_2As_2 is unusual in that its Fermi surface does not consist of quasi-nested electron and hole pockets. Here we report measurements of the temperature dependent London penetration depth of very clean crystals of this compound with residual resistivity ratio > 1200 . We show that the superfluid density at low temperatures exhibits a strong linear-in-temperature dependence which implies that there are line nodes in the energy gap on the large zone-centered hole sheets. The results indicate that KFe_2As_2 is an unconventional superconductor with strong electron correlations.

I. INTRODUCTION

The discovery of high transition temperature (T_c) iron-based superconductors (IBS) raises fundamental questions about origin of superconductivity.¹ The microscopic pairing interactions which give rise to superconductivity are intimately related to the structure of the superconducting energy gap which may be probed experimentally by studying the nature of the low-energy quasiparticle excitations. In particular, the presence of nodes in the energy gap signals an unconventional pairing mechanism, and the position of the nodes can be a strong guide as the exact form of the pairing interaction $V_{kk'}$.

Based on analyses of spin-fluctuation mediated pairing models, several different gap structures have been proposed.²⁻⁶ The rich variety of possible pairing states has as its origin the unusual multiband electronic structure of the IBS. In most IBS there are disconnected quasi-two-dimensional hole and electron Fermi-surface sheets. The former are centered on the Γ point in the Brillouin zone and the latter at the zone corner.¹ Strong scattering between the electron and hole sheets, corresponding to a wavevector $\mathbf{q} \sim (\pi, \pi)$ leads to a nodeless gap with sign change between the hole and electron sheets (nodeless s_{\pm} state).^{2,3} However, if in addition to this there is strong low \mathbf{q} scattering this can stabilize a state with nodes in the electron and/or hole bands with either s or d -wave symmetry.³⁻⁵ c -axis Fermi-surface dispersion could also generate horizontal line nodes.^{5,7,8}

Thus far experimental studies have given evidence for two distinct types of nodal structure in IBS:¹ one is nodeless but may have significant anisotropy⁹⁻¹⁴ and the other has line nodes.¹⁵⁻¹⁹ The former fully gapped state seems consistent with the nodeless s_{\pm} state, but it may also be explained by the conventional s (s_{++}) state.²⁰ For the latter case, strong evidence of nodal lines has been obtained from the penetration depth and thermal conductivity measurements in the compensated metals LaFePO ($T_c = 6$ K)¹⁵⁻¹⁷ and $\text{BaFe}_2(\text{As,P})_2$ ($T_c = 30$ K).¹⁸ In both materials, recent studies^{17,21,22} suggest that the nodes are most likely located on the electron bands

near the zone corner of the Brillouin Zone, and that the hole bands centered at the Γ point remains fully gapped.

To uncover how the superconducting gap structure is related to the microscopic pairing in IBS, studies of KFe_2As_2 may be particularly instructive. This superconductor has a relatively low $T_c \simeq 3$ K and is the end member of the $(\text{Ba}_{1-x}\text{K}_x)\text{Fe}_2\text{As}_2$ series. Unlike most other IBS where the volumes of the electron and hole sheets are roughly equal, in KFe_2As_2 the volumes differ by one electron per unit cell.²³ This causes a sub-

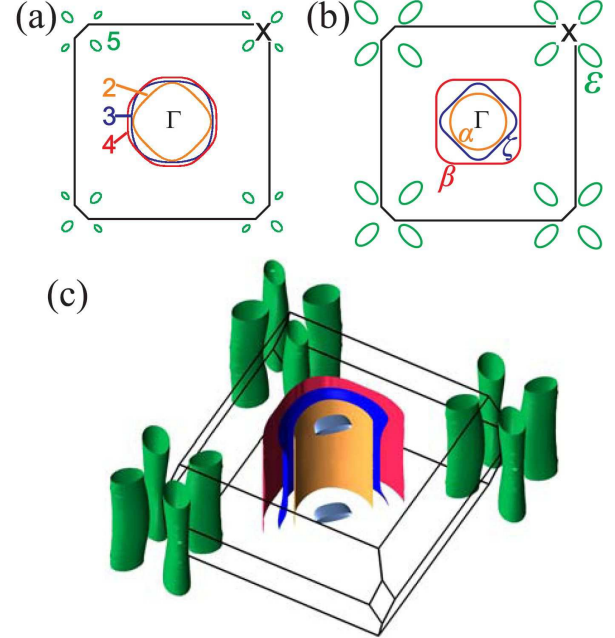


FIG. 1. (Color online). The Fermi surface of KFe_2As_2 (labels in correspond to Table I). (a) 2D cross-sectional representation of our band-structure calculations (note the pillow surface from band 1 does not appear in this cut). (b) Schematic cross-section with shapes of the various pockets determined by dHvA²³ and ARPES⁴³ experiments. (c) 3D view of the DFT calculated Fermi surface with bands energies shifted to best fit the dHvA frequencies.⁴⁶

stantial change in the Fermi surface topology. As shown in Fig. 1, the ubiquitous X centered electron sheets are replaced by small quasi-two-dimensional hole-like tubes which do not nest at all with the Γ -centered hole sheets. If nesting does play an important role in the superconductivity of the high- T_c IBS then the nature of the superconducting state should be quite different in KFe_2As_2 . It is also intriguing that the electronic specific heat is quite large ($\gamma = 93 \text{ mJ/K}^2\text{mol}$) compared with other IBS,²⁴ suggesting the importance of electron correlations in KFe_2As_2 . In this paper, we report measurements of the temperature dependent penetration depth of KFe_2As_2 which shows that this material has well formed line nodes located in the Γ -centered hole bands.

II. EXPERIMENTAL METHODS

The temperature dependence of the magnetic penetration depth $\lambda(T)$ was measured using a self-resonant tunnel-diode oscillator which was mounted in a dilution refrigerator.¹⁵ The sample (approximate dimensions $0.2 \times 0.2 \times 0.02 \text{ mm}^3$) is mounted on a sapphire rod, the other end of which is glued to a copper block on which a RuO_2 thermometer is mounted. The sample and rod are placed inside a solenoid which forms part of the resonant tank circuit which operates at $\sim 14 \text{ MHz}$. The RF field within this solenoid is estimated to be $< 10^{-6} \text{ T}$ so that the sample is always in the Meissner state. DC fields are screened to a similar level using a mu-metal can. Changes in the resonant frequency are directly proportional to changes in the magnetic penetration depth as the temperature of the sample is varied. The calibration factor is determined from the geometry of the sample, and the total perturbation to the resonant frequency due to the sample, found by withdrawing the sample from the coil at low temperature.²⁵ The sapphire sample holder has a very small paramagnetic background signal which varies $\sim 1/(T + \theta)$ which corresponds to a change of $\sim 0.4 \text{ nm}$ in λ of our samples between 100 mK and 200 mK . This is around ten times smaller than the signal from the sample and was subtracted. The ac magnetic field is applied parallel to the c axis so that the shielding currents flow in the ab -plane. To avoid degradation of the crystals due to reaction with moisture in the air, we cleaved the crystals on all six sides while they were coated in a thick layer of grease. The measurements were done just after the cleavage without exposure in air. The relatively sharp superconducting transitions found in the frequency shift of the oscillator as well as in the specific heat measured after the penetration depth measurements [inset of Fig. 4] indicate that our procedure does not reduce the sample quality.

The single crystals were grown by a self-flux method which will be described in detail elsewhere.²⁶ The temperature dependence of dc resistivity $\rho(T)$ was measured by the standard 4-probe method. Au contacts were evaporated after Ar plasma cleaning of the surface, which give contact resistance less than 1Ω . The voltage contacts have finite widths which gives uncertainty of the absolute value of ρ up to $\sim 22\%$, but the temperature dependence is not affected by this uncertainty.

In order to determine the bulk homogeneity of the super-

conductivity in our samples, specific heat measurements were performed on the same single crystal sample as was used for the penetration depth measurements. Because of the small size of these samples (mass $\sim 4 \mu\text{g}$), a modulated temperature method was used.²⁷ Briefly, the sample is glued to a $10 \mu\text{m}$ diameter chromel-constantan thermocouple and heated with modulated light from a room temperature LED via an optical fibre. This method has a high sensitivity but has poor absolute accuracy, so the values are quoted in arbitrary units.

III. RESULTS AND DISCUSSION

Dc resistivity $\rho(T)$ measurements show that our crystals are extremely clean with the residual resistivity ratio $RRR = \rho(300 \text{ K})/\rho_0$ of 1280 [Figs. 2(a) and (b)]. The low-temperature normal-state $\rho(T)$ follows the Fermi-liquid dependence $\rho_0 + AT^2$ with $A = 0.030(7) \mu\Omega\text{cm/K}^2$, and the residual resistivity ρ_0 is estimated by extrapolation. We note our data is not consistent with the non-Fermi-liquid $T^{1.5}$ behavior reported by Dong *et al.*,²⁸ but is consistent with another previous report.²⁹ The obtained relatively large A value follows the Kadowaki-Woods relation $A = a_{\text{KW}}\gamma^2$,³⁰ with $a_{\text{KW}} \approx 10^{-5} \mu\Omega\text{cm}(\text{Kmol/mJ})^2$, indicating that strongly

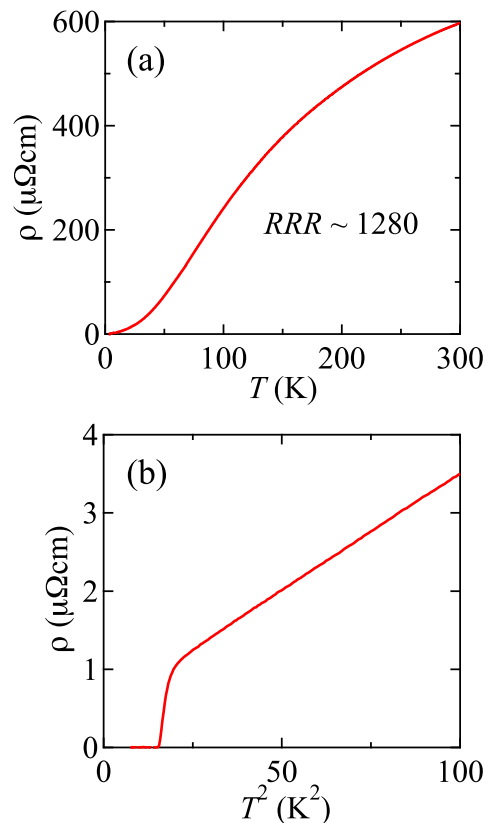


FIG. 2. (Color online). (a) Temperature dependence of in-plane resistivity $\rho(T)$ in a single crystal of KFe_2As_2 . (b) The same data plotted against T^2 below 10 K .

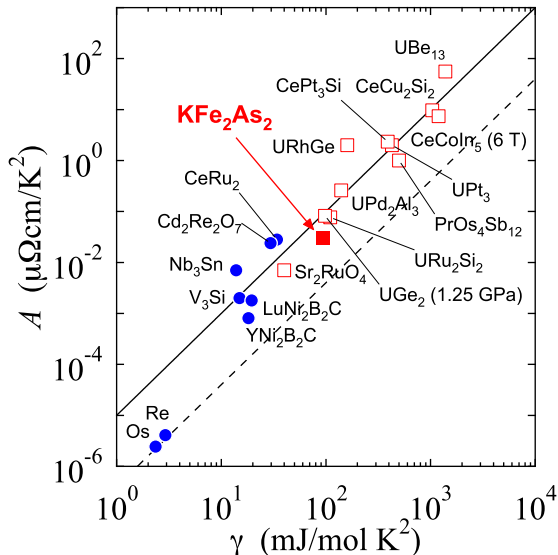


FIG. 3. (Color online). Coefficient A vs Sommerfeld constant γ (Kadowaki-Woods plot³⁰) for various superconductors showing the Fermi-liquid AT^2 dependence of $\rho(T)$. Blue circles are for s -wave superconductors, while red squares are for unconventional superconductors with nodes in the gap.⁴⁷ The lines represent $A = a_{KW}\gamma^2$, with $a_{KW} = 10^{-5}$ (solid line) and $4 \times 10^{-7} \mu\Omega\text{cm}(\text{Kmol}/\text{mJ})^2$ (dashed line).

correlated electrons with large mass are responsible for the Fermi-liquid T^2 dependence. As demonstrated in Fig. 3, KFe_2As_2 is at the edge of heavy-fermion superconductors with nodes in the energy gap which are widely believed to have unconventional mechanisms of superconductivity.³¹

Figure 4 shows the low-temperature variation of the change in the penetration depth $\Delta\lambda(T) = \lambda(T) - \lambda(0)$ in two samples. In both samples a strong T -linear dependence is observed over a wide temperature range of $0.1 \lesssim T/T_c \lesssim 0.25$. Such a strong T -linear dependence is distinctly different from the exponential dependence expected in the fully-gapped superconducting state and is instead consistent with gap with well-developed line nodes.³² This is in contrast to power law behaviors with exponents close to 2 which could be consistent either with nodal behavior in the dirty limit or with strong impurity scattering in e.g. the intrinsically fully gapped s_{\pm} state.³² Evidence for line nodes in this compound has also been found in NMR, specific heat³³ and thermal conductivity²⁸ measurements.

Deviations from the T -linear behavior of $\lambda(T)$ are observed at the lowest temperatures which are likely due to a finite zero-energy density of states created by a small amount of impurity scattering. When impurity scattering is present in superconductors with line nodes, the low-temperature $\Delta\lambda(T)$ changes from T to T^2 , which can be described by the empirical formula $\Delta\lambda(T) \propto T^2/(T + T^*)$.³⁴ A fit to this formula [solid lines in Fig. 4] gives $T^* \approx 0.3$ K for sample 1 and $T^* \approx 0.5$ K for sample 2, which indicates relatively small levels of disorder in these crystals.

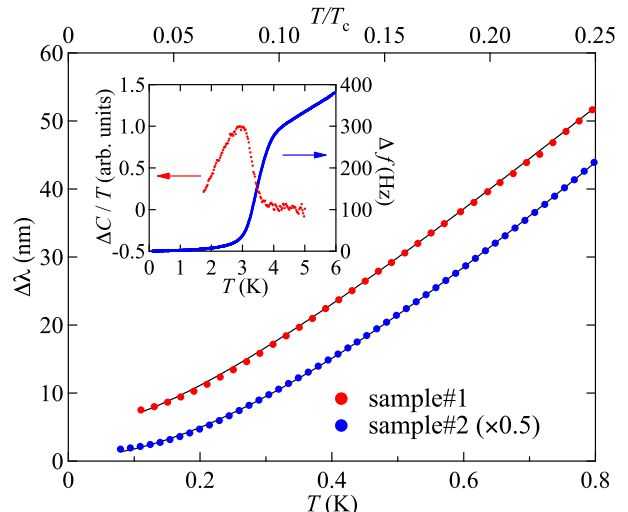


FIG. 4. (Color online). Change in the penetration depth $\Delta\lambda(T)$ at low temperatures in two samples. The data are shifted vertically for clarity. Inset shows the frequency shift Δf of the oscillator containing sample 1, and relative change in the specific heat divided by temperature $\Delta C/T$ in the same sample.

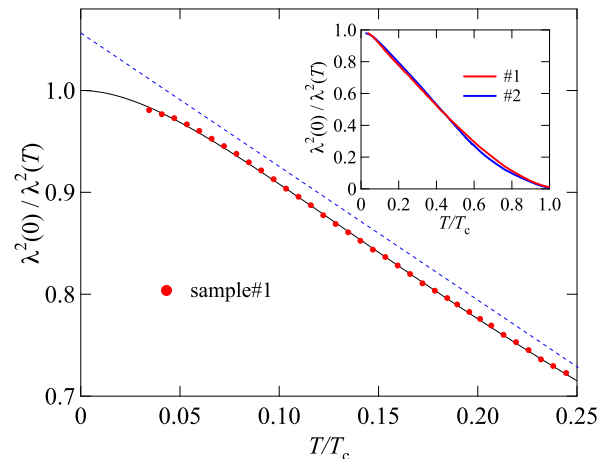


FIG. 5. (Color online). Normalized superfluid density at low temperatures follows a T -linear dependence (dashed line). We used $\lambda(0) = 260$ nm estimated from the Fermi-surface parameters. The solid lines are fits to the empirical formula involving the impurity scattering in superconductors with line nodes (see text). Inset compares the normalized superfluid density data for the two samples. To account for the factor of two difference in the slope of $\Delta\lambda(T)$ at low temperatures, we used the doubled $\lambda(0)$ value for sample 2.

der in these crystals.

Although the temperature dependence of λ is consistent between samples the absolute values of $d\lambda/dT$ differ by a factor two. Although our calibration procedure linking the measured frequency shift to the change in λ has proved to be highly accurate (~ 5 -10%) for polycrystalline elemental test samples and high- T_c cuprate superconductors such as $\text{YBa}_2\text{Cu}_3\text{O}_{7-\delta}$

TABLE I. Contributions of each band to the normalized superfluid density $\lambda^2(0)/\lambda^2(T)$ evaluated from DFT band structure calculations as well as the dHvA measurements.²³ m_e is the free electron mass.

Sheet	From DFT calculations				From dHvA			
	# holes	DOS (eV)	ω_p (eV)	$\frac{\omega_p^2}{(\omega_p^2)_{\text{total}}} (\%)$	name	# holes	$\frac{m^*}{m_e}$	$\frac{\omega_p^2}{(\omega_p^2)_{\text{total}}} (\%)$
1 (pillow at Z)	0.002	0.055	0.16	0.4	–	–	–	–
2 (inner tube at Γ)	0.258	1.11	1.466	32	α	0.17	6	31
3 (middle tube at Γ)	0.342	1.48	1.3959	29	ζ	0.26	13	23
4 (outer tube at Γ)	0.390	1.52	1.5098	34	β	0.48	18	31
5 (tubes near X)	0.009	1.328	0.55	5	ε	0.09	7	15
total	1.00	5.494	2.577	100		1.0		100

(Refs. 25 and 35), in some cases where there is large surface roughness of the cut edges $\Delta\lambda$ may be overestimated. We obtain almost identical temperature dependence of the normalized superfluid density $\lambda^2(0)/\lambda^2(T)$ if we use the doubled $\lambda(0)$ value for sample 2 [inset of Fig. 5]. This indicates that only the calibration factor has a factor of two differences between the two samples and the whole temperature dependence is quite reproducible. A similar effect was found in LaFePO.¹⁵ The lower value found for sample 1 is likely to be more representative of the intrinsic value although in LaFePO the values of $\Delta\lambda$ found by scanning SQUID spectrometry¹⁶ were around a factor two smaller than our lowest estimate.¹⁵ This has implications for our calculations of the superfluid density as will be discussed below.

To evaluate the normalized superfluid density $n_s(T)/n_s(0) = \lambda^2(0)/\lambda^2(T)$, we need the value of $\lambda(0)$, which we cannot measure directly in our experiment. Recent small-angle neutron scattering (SANS) measurements³⁶ estimate $\lambda(T = 55 \text{ mK}) \approx 200 \text{ nm}$ and μSR measurements³⁷ give $\lambda(T_c/2) \approx 280 \text{ nm}$ which also suggests $\lambda(0) \sim 200 \text{ nm}$. These values are close to the $\lambda(0)$ values calculated from the Fermi surface parameters [see Table I]. Regardless of the choice of $\lambda(0)$ value within the uncertainties, the obtained temperature dependence of $n_s(T)$ shows a T -linear behavior over a even wider range of T than $\lambda(T)$ itself [Figs. 5 and 6]. This is expected because the $1 - \alpha(T/T_c)$ dependence of $n_s(T)/n_s(0)$ gives $\Delta\lambda(T)/\lambda(0) = \frac{1}{2}\alpha(T/T_c) + \frac{3}{8}\alpha^2(T/T_c)^2 + \dots$ which leads to slightly concave (superlinear) temperature dependence for the penetration depth as we observed.

In order to proceed with a more quantitative analysis of our results we have estimated the contribution of each of the Fermi surface sheets to the total superfluid density. As a first approach we have calculated the band structure of KFe_2As_2 using density functional theory (DFT) using the WIEN2K package³⁸ and the experimental lattice constants and internal positions.³⁹ 4×10^5 k -points (in the full Brillouin zone) were used for the calculations of plasma frequencies ω_p , Fermi surface volumes and sheet specific density of states (DOS) which are reported in Table I. The Fermi surface topology and band masses are very similar to those reported previously²⁹ [Fig. 1]. The calculated total DOS and ω_p correspond to the Sommerfeld constant $\gamma = 13.0 \text{ mJ/K}^2\text{mol}$ and $\lambda(0) = 76.6 \text{ nm}$, respectively. The experimentally observed $\gamma = 93 \text{ mJ/K}^2\text{mol}$ (Ref. 24) implies a renormalization of 7.2 in the total den-

sity of states at the Fermi level. Assuming that the superfluid density is renormalized by the same factor leads to $\lambda(0)$ being increased to 205 nm. We note that in Galilean-invariant (translation-invariant) systems like liquid ^3He the Fermi liquid corrections to λ cancel in the zero temperature limit.⁴⁰ However, in crystalline solids this cancellation is thought not to occur⁴¹ and indeed in heavy-Fermion systems a reduction in superfluid density consistent with the thermodynamic mass enhancement is observed.⁴²

Although the general features of this Fermi surface calculation are confirmed by angle-resolved photoemission spectroscopy (ARPES)⁴³ and de Haas-van Alphen (dHvA) measurements,²³ the exact size of the various sheets and their warping are not. Also, dHvA measurements show that the mass renormalization effects vary between the different sheets. So as a second approach we estimate the contribution of the various sheets to the superfluid density directly from the dHvA measurements, assuming each sheet is a simple two dimensional cylinder. As the largest β sheet [see Fig. 1] was not observed by dHvA, we estimate its volume from the total hole number constraint and its mass by using the measured specific heat. Note that for sheets with more than one extremal dHvA orbit we have taken the average. Also we have ignored any possible contribution from the small pillow sheet (band 1). The contribution of each sheet to the superfluid density were then calculated using $\lambda^{-2} = \mu_0 e^2 n_H / m^* = \omega_p^2 / c^2$, where n_H and m^* are the hole density and effective mass for each sheet. From this we obtain a total superfluid density which corresponds to $\lambda(0) = 260 \text{ nm}$. The fact that this procedure and the direct calculation from the band structure (including renormalization) give values of $\lambda(0)$ which compare favorable to the direct measurements by μSR and SANS gives us confidence in the accuracy of the result. A key result from this analysis is that the contribution of the ε band near the X point is small. It contributes only up to $\sim 15\%$ of the total superfluid density.

The temperature dependence of the normalized superfluid density $\rho_s = \lambda^2(0)/\lambda^2(T)$ is plotted in Fig. 6. Here we have used values of $\lambda(0)$ which encompass the above estimates as well as a factor of 2 larger value in case our values of $\Delta\lambda(T)$ are overestimated because of remaining surface roughness in sample 1. These plots show that the superfluid density at $T = T_c/3$ does not exceed $\sim 75\%$ of the zero-temperature value which indicates that the nodes are located on at least one of the Γ -centered bands which have large contributions to the

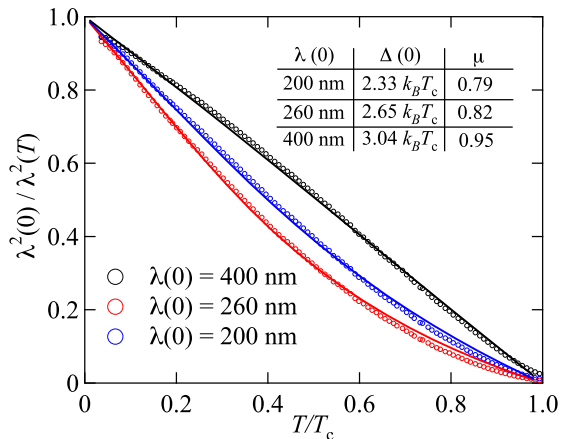


FIG. 6. (Color online). Normalized superfluid density obtained by using representative values of $\lambda(0)$. The lines are the fits to the nodal-gap model with parameters indicated in the figure.

superfluid density.

In a nodal superconductor a rapid decrease of superfluid density with increasing temperature is indicative of a small value of the gap slope near the nodes $\mu\Delta_0 = 1/d\Delta/d\phi|_{\text{node}}$ (in a simple d -wave model⁴⁴ for $T \ll T_c$: $\rho_s(T) \simeq 1 - 4 \ln 2/\mu\Delta_0$). The presence of multiple Fermi surface sheets complicates the analysis in the present case, but it is reasonable to approximately model the gaps and Fermi velocity values on the different sheets by globally averaged values of μ and Δ . We then approximate the variation of the gap with in-plane Fermi surface angle ϕ by $\Delta(\phi) = \min(\mu\Delta_0\phi, \Delta_0)$.⁴⁴ We note that for $\mu = 2$ this produces a very similar form of $\rho_s(T/T_c)$ to the more usual d -wave form $\Delta(\phi) = \Delta_0 \cos(2\phi)$. An alternative way of modelling the gap would be to add higher harmonics to this lowest order d -wave form. However, this would introduce more fitting parameters if more than one extra harmonic was required. In the weak-coupling limit, μ is the only free parameter in this model as the temperature dependent gap can be calculated self-consistently.⁴⁴ Here however, we allow for possible strong-coupling corrections to Δ_0 and leave this as a free parameter, fixing the temperature dependence of Δ to its weak-coupling d -wave form.

As shown in Fig. 6, we find this model fits our data well for all assumed values of $\lambda(0)$. There is strong covariance between the two parameters μ and Δ_0 because the low T slope is determined only by the product $\mu\Delta_0$ whereas the variable ratio μ/Δ_0 influences the higher T behavior only weakly. We

find the data can also be reasonably well fitted by the inclusion of a second isotropic gap accounting for $\sim 30\%$ of the total, but the large reduction of ρ_s at low temperatures cannot be reproduced if we assume that only the ε tubes have line nodes as they only contribute $\sim 15\%$ to the total superfluid density. This reaffirms our conclusion that nodes must be present on the Γ centered hole bands, although there is a possibility that some of the sheets could be fully gapped.

As demonstrated in Fig. 3, in superconductors with strong electron correlations where the A and γ values are strongly enhanced, Cooper pairs with finite angular momentum (p , d -wave, etc.) are favorable as these states with small probabilities in small pair distances reduce the Coulomb repulsion.³¹ Our results indicate that KFe_2As_2 with γ and A values comparable to some heavy-fermion superconductors has well-developed line nodes in the zone-centered large bands. This implies that the electron correlations play an important role in this compound and that an electronic (non-phononic) pairing mechanism is needed to overcome the Coulomb repulsion. Since the Γ -centered sheets in KFe_2As_2 are relatively large, it is likely that the intra-band spin-fluctuations are important to create the sign change inside these bands, which gives rise to line nodes. Recent theoretical calculations⁴⁵ reveal that the spin susceptibility in heavily hole doped system has relatively weak momentum dependence, which suggests the relative importance of scattering vectors other than $\mathbf{q} \sim (\pi, \pi)$.

IV. CONCLUSIONS

In summary, our results indicating line nodes in the Γ -centered bands in KFe_2As_2 are consistent with d -wave or horizontal nodal state. This is different both from the nodeless states found in $(\text{Ba},\text{K})\text{Fe}_2\text{As}_2$ (Refs. 9 and 11) and from the nodal s state with nodes in the electron bands³⁻⁵ which may be the case in $\text{BaFe}_2(\text{As},\text{P})_2$.^{18,21,22} How this difference is linked to the changes in the Fermi surface will be an important clue towards a microscopic mechanism of superconductivity in iron-based superconductors.

ACKNOWLEDGMENTS

We thank discussions with D. Broun, E.M. Forgan, S. Kasahara, H. Kawano-Furukawa, K. Kuroki, K. Ohishi, and T. Terashima. This work is supported by KAKENHI from JSPS, Grant-in-Aid for GCOE program “The Next Generation of Physics, Spun from Universality and Emergence” from MEXT, Japan, and EPSRC in the UK.

¹ K. Ishida, Y. Nakai, and H. Hosono, J. Phys. Soc. Jpn. **78**, 062001 (2009).

² I. I. Mazin, D. J. Singh, M. D. Johannes, and M. H. Du, Phys. Rev. Lett. **101**, 057003 (2008).

³ K. Kuroki, H. Usui, S. Onari, R. Arita, and H. Aoki, Phys. Rev. B **79**, 224511 (2009).

⁴ A. V. Chubukov, M. G. Vavilov, and A. B. Vorontsov, Phys. Rev. B **80**, 140515(R) (2009).

⁵ S. Graser, A. F. Kemper, T. A. Maier, H.-P. Cheng, P. J. Hirschfeld, and D. J. Scalapino, New J. Phys. **11**, 025016 (2009); arXiv:1003.0133.

⁶ H. Ikeda, R. Arita, and J. Kuneš, Phys. Rev. B **81**, 054502 (2010).

- ⁷ L. Craco and M. S. Laad, Phys. Rev. B **80**, 054520 (2009).
- ⁸ K. Kuroki (private communications).
- ⁹ K. Hashimoto, T. Shibauchi, T. Kato, K. Ikada, R. Okazaki, H. Shishido, M. Ishikado, H. Kito, A. Iyo, H. Eisaki, S. Shamoto, and Y. Matsuda, Phys. Rev. Lett. **102**, 017002 (2009); K. Hashimoto, T. Shibauchi, S. Kasahara, K. Ikada, S. Tonegawa, T. Kato, R. Okazaki, C. J. van der Beek, M. Konczykowski, H. Takeya, K. Hirata, T. Terashima, and Y. Matsuda, Phys. Rev. Lett. **102**, 207001 (2009).
- ¹⁰ L. Malone, J. D. Fletcher, A. Serafin, and A. Carrington, N. D. Zhigadlo, Z. Bukowski, S. Katrych, and J. Karpinski, Phys. Rev. B **79**, 140501(R) (2009).
- ¹¹ H. Ding, P. Richard, K. Nakayama, T. Sugawara, T. Arakane, Y. Sekiba, A. Takayama, S. Souma, T. Sato, T. Takahashi, Z. Wang, X. Dai, Z. Fang, G. F. Chen, J. L. Luo, and N. L. Wang, Europhys. Lett. **83**, 47001 (2008).
- ¹² H. Kim, R. T. Gordon, M. A. Tanatar, J. Hua, U. Welp, W. K. Kwok, N. Ni, S. L. Bud'ko, P. C. Canfield, A. B. Vorontsov, and R. Prozorov, arXiv:1003.2959 (unpublished); R. T. Gordon, R. T. Gordon, H. Kim, M. A. Tanatar, R. Prozorov, and V. G. Kogan, Phys. Rev. B **81**, 180501(R) (2010), and references therein.
- ¹³ M. Yashima, H. Nishimura, H. Mukuda, Y. Kitaoka, K. Miyazawa, P. M. Shirage, K. Kiho, H. Kito, H. Eisaki, and A. Iyo, J. Phys. Soc. Jpn. **78**, 103702 (2009).
- ¹⁴ X. G. Luo, M. A. Tanatar, J.-Ph. Reid, H. Shakeripour, N. Doiron-Leyraud, N. Ni, S. L. Bud'ko, P. C. Canfield, Huiqian Luo, Zhaosheng Wang, Hai-Hu Wen, R. Prozorov, and Louis Taillefer, Phys. Rev. B **80**, 140503(R) (2009); M. A. Tanatar, J.-Ph. Reid, H. Shakeripour, N. Doiron-Leyraud, N. Ni, S. L. Bud'ko, P. C. Canfield, Huiqian Luo, Zhaosheng Wang, Hai-Hu Wen, Ruslan Prozorov, and Louis Taillefer, Phys. Rev. Lett. **104**, 067002 (2010); L. Ding, J. K. Dong, S. Y. Zhou, T. Y. Guan, X. Qiu, C. Zhang, L. J. Li, X. Lin, G. H. Cao, Z. A. Xu and S. Y. Li, New J. Phys. **11**, 093018 (2009).
- ¹⁵ J. D. Fletcher, A. Serafin, L. Malone, J. G. Analytis, J.-H. Chu, A. S. Erickson, I. R. Fisher, and A. Carrington, Phys. Rev. Lett. **102**, 147001 (2009).
- ¹⁶ C. W. Hicks, T. M. Lippman, M. E. Huber, J. G. Analytis, J.-H. Chu, A. S. Erickson, I. R. Fisher, and K. A. Moler, Phys. Rev. Lett. **103**, 127003 (2009).
- ¹⁷ M. Yamashita, N. Nakata, Y. Senshu, S. Tonegawa, K. Ikada, K. Hashimoto, H. Sugawara, T. Shibauchi, and Y. Matsuda, Phys. Rev. B **80**, 220509(R) (2009).
- ¹⁸ K. Hashimoto, M. Yamashita, S. Kasahara, Y. Senshu, N. Nakata, S. Tonegawa, K. Ikada, A. Serafin, A. Carrington, T. Terashima, H. Ikeda, T. Shibauchi, and Y. Matsuda, Phys. Rev. B **81**, 220501(R) (2010).
- ¹⁹ Y. Nakai, T. Iye, S. Kitagawa, K. Ishida, S. Kasahara, T. Shibauchi, Y. Matsuda, and T. Terashima, Phys. Rev. B **81**, 020503(R) (2010).
- ²⁰ H. Kontani and S. Onari, Phys. Rev. Lett. **104**, 157001 (2010).
- ²¹ J. S. Kim, P. J. Hirschfeld, G. R. Stewart, S. Kasahara, T. Shibauchi, T. Terashima, and Y. Matsuda, Phys. Rev. B **81**, 214507 (2010).
- ²² T. Shimojima *et al.* (unpublished).
- ²³ T. Terashima, M. Kimata, N. Kurita, H. Satsukawa, A. Harada, K. Hazama, M. Imai, A. Sato, K. Kihou, C.-H. Lee, H. Kito, H. Eisaki, A. Iyo, T. Saito, H. Fukazawa, Y. Kohori, H. Harima, and S. Uji, J. Phys. Soc. Jpn. **79**, 053702 (2010).
- ²⁴ H. Fukazawa *et al.* (unpublished).
- ²⁵ R. Prozorov, R.W. Giannetta, A. Carrington, and F. M. Araujo-Moreira, Phys. Rev. B **62**, 115 (2000).
- ²⁶ K. Kihou, T. Saito, S. Ishida, Y. Tomioka, H. Fukazawa, Y. Kohori, T. Ito, S. Uchida, A. Iyo, C. H. Lee, and H. Eisaki (unpublished).
- ²⁷ A. Carrington, C. Marcenat, F. Bouquet, D. Colson, A. Bertinotti, J. F. Marucco, and J. Hammann, Phys. Rev. B **55**, R8674 (1997).
- ²⁸ J. K. Dong, S. Y. Zhou, T. Y. Guan, H. Zhang, Y. F. Dai, X. Qiu, X. F. Wang, Y. He, X. H. Chen, and S. Y. Li, Phys. Rev. Lett. **104**, 087005 (2010).
- ²⁹ T. Terashima, M. Kimata, H. Satsukawa, A. Harada, K. Hazama, S. Uji, H. Harima, G.-F. Chen, J.-L. Luo, and N.-L. Wang, J. Phys. Soc. Jpn. **78**, 063702 (2009).
- ³⁰ K. Kadawaki and S. B. Woods, Solid State Commun. **58**, 507 (1986).
- ³¹ P. Monthoux, D. Pines, and G. G. Lonzarich, Nature **450**, 1177 (2007).
- ³² A. B. Vorontsov, M. G. Vavilov, and A. V. Chubukov, Phys. Rev. B **79**, 140507(R) (2009); Y. Bang, EPL **86**, 47001 (2009).
- ³³ H. Fukazawa, Y. Yamada, K. Kondo, T. Saito, Y. Kohori, K. Kuga, Y. Matsumoto, S. Nakatsuji, H. Kito, P.M. Shirage, K. Kihou, N. Takeshita, C.-H. Lee, A. Iyo, and H. Eisaki, J. Phys. Soc. Jpn. **78**, 083712 (2009).
- ³⁴ P. J. Hirschfeld, and N. Goldenfeld, Phys. Rev. B **48**, 4219 (1993).
- ³⁵ A. Carrington, F. Manzano, R. Prozorov, R.W. Giannetta, N. Kameda, and T. Tamegai, Phys. Rev. Lett. **86**, 1074, (2001).
- ³⁶ H. Kawano-Furukawa, C. J. Powell, J. S. White, R. W. Heslop, A. S. Cameron, E. M. Forgan, K. Kihou, C. H. Lee, A. Iyo, H. Eisaki, T. Saito, H. Fukazawa, Y. Kohori, R. Cubitt, C. D. Dewhurst, J. L. Gavilano and M. Zolliker, arXiv:1005.4468 (unpublished).
- ³⁷ K. Ohishi *et al.* (unpublished).
- ³⁸ P. Blaha, K. Schwarz, G. Madsen, D. Kvasnicka, and J. Luitz, An Augmented Plane Wave+Local Orbitals Program for Calculating Crystal Properties (Karlheinz Schwarz, Techn. Universitat Wien, Austria, 2001).
- ³⁹ S. Rozca, and H. U. Schuster, Z. Naturforsch. B **36**, 1668 (1981). $a = 3.841 \text{ \AA}$, $c = 13.861 \text{ \AA}$, and $z_{As} = 0.3525$.
- ⁴⁰ A. J. Leggett, Phys. Rev. **140**, A1869 (1965).
- ⁴¹ C. M. Varma, K. Miyake, and S. Schmitt-Rink, Phys. Rev. Lett. **57**, 626 (1986).
- ⁴² F. Gross, B. S. Chandrasekhar, D. Einzel, K. Andres, P. J. Hirschfeld, H. R. Ott, J. Beuers, Z. Fisk, and J. L. Smith, Z. Phys. B: Cond. Matt. **64**, 175 (1986).
- ⁴³ T. Sato, K. Nakayama, Y. Sekiba, P. Richard, Y.-M. Xu, S. Souma, T. Takahashi, G. F. Chen, J. L. Luo, N. L. Wang, and H. Ding, Phys. Rev. Lett. **103**, 047002 (2009).
- ⁴⁴ D. Xu, S. K. Yip, and J. A. Sauls, Phys. Rev. B **51**, 16233 (1995).
- ⁴⁵ H. Ikeda, R. Arita, and J. Kuneš, arXiv:1002.4471 (unpublished).
- ⁴⁶ Rigid band energy shifts of 0, +20, -120, +50, +30 meV for bands 1-5 respectively were applied to best reproduce the observed de Haas-van Alphen effect measurement frequencies reported in Ref. 23. The lowest frequencies (ϵ_l , ϵ_h in the notation of Ref. 23) were assigned to the corner hole pockets (band 5). With this energy shift the band mass of these pockets increases to $1.7 m_e$ so the enhancement factor $m^*/m_b = 3.5$ rather than ~ 20 for the unshifted bands.²³ This enhancement then close to the values for the other sheets. No orbits corresponding to those predicted for band 1 were observed experimentally, so this was left unshifted in the figure, but in reality may not be present.
- ⁴⁷ Y. Kasahara, Y. Kasahara, Y. Shimono, T. Shibauchi, Y. Matsuda, S. Yonezawa, Y. Muraoka, and Z. Hiroi, Phys. Rev. Lett. **96**, 247004 (2006).